152-dB Dynamic Range With a Large-Area Custom-Technology Single-Photon Avalanche Diode

Francesco Ceccarelli ID, Giulia Acconcia, Ivan Labanca, Angelo Gulinatti, *Member, IEEE*, Massimo Ghioni, *Senior Member, IEEE*, and Ivan Rech, *Senior Member, IEEE*

***Abstract*— In this letter, we demonstrate a dynamic range as high as 152 dB with a detection head based on a single-photon avalanche diode (SPAD). This result has been attained by exploiting two key factors: on one hand, the low dark count rate (9 cps) of a custom-technology SPAD; and on the other hand, the maximum count rate (120 Mcps) achievable with a new generation active quenching circuit and an optimized assembly of the system. To the best of our knowledge, this is the highest dynamic range reported so far in the literature for a SPAD. Even more important, this value has been attained without sacrificing other detector parameters, such as active area diameter (50 µm), photon detection efficiency (50% at 550-nm wavelength), and afterpulsing probability (2%).**

***Index Terms*— Single-photon avalanche diode (SPAD), high dynamic range, high count rate, single-photon counting.**

I. Introduction

SINGLE-PHOTON avalanche diodes (SPADs) are nowadays recognized as the detectors of choice for many applications requiring single-photon sensitivity. Their use encompasses applications as diverse as fluorescence lifetime imaging (FLIM) [1], single-molecule fluorescence spectroscopy [2], and quantum key distribution (QKD) [3]. Typical requirements are large active area, low dark count rate (DCR), high photon detection efficiency (PDE) and low photon timing jitter. However, some applications are also influenced by the dynamic range (DR), i.e. by the ratio between the maximum and the minimum number of photons detectable by the device in a fixed integration window. A high DR is of paramount importance for example in laser scanning fluorescence microscopy, when the scene to be acquired presents structures with a large contrast (e.g. in neuronal imaging) [4].

In a SPAD, two different mechanisms limit the attainable DR. On one hand, the minimum number of detectable photons is limited by the dark counts, whose statistical fluctuations constitute the detector noise. On the other hand, the upper limit is set by the dead time, i.e. the time required by the electronics to quench the avalanche and reset the initial bias conditions. The best DRs reported in literature to date have been attained by Eisele *et al.* [5] and by Bronzi *et al.* [6] with SPADs fabricated by using a CMOS technology (CMOS SPAD). This approach allows the integration of the detector and quenching circuitry on the same silicon chip and therefore a minimization of the parasitics, with obvious advantages in terms of the maximum count rate. However, the tight constraints set by the use of a standard CMOS technology do not allow for a complete optimization of the detector design, resulting either in high DCR [5], or in low detection efficiency at red/near-infrared wavelengths [6], [7]. This prevents or limits the use of CMOS SPADs in certain applications.

On the other hand, the use of a custom technology for the fabrication of the SPAD detectors allows one to attain a combination of high PDE, low DCR and low timing jitter [8], [9] mandatory for applications like single-molecule Förster resonance energy transfer (smFRET) [2]. However, being the technology specialized for the detector, active quenching circuit (AQC) and possible avalanche readout must be fabricated in one or more separate chips [10], with negative effects in terms of parasitic components and therefore of DR.

In the past we already demonstrated that a high DR of 141 dB can be achieved with a fully parallel array of 8×8 custom SPADs [11]. In fact, the array can be used as a single macro-pixel in which the detection of a photon temporarily turns off only the corresponding SPAD of the array, while the others remain fully operative. This produces a reduced effective dead time that increases the maximum count rate to more than 1 Gcps. Of course this result comes at the expenses of the increased complexity and cost associated with the use of an array. Moreover, the noise is higher as the DCRs of the single pixels add up. Finally, an array of micro-lenses, that focuses the incoming light on the SPADs active areas, is needed to avoid the losses due to the dead space between pixels. Therefore cost, simplicity or low noise requirements suggest that for some applications the use of a single-pixel SPAD would be preferable compared to an array.

In this letter we show that, thanks to the use of a new generation AQC and an optimized assembly, we can attain a record DR of 152 dB with a low-noise custom-SPAD, without sacrificing other performance like PDE or afterpulsing.

II. Detection Head

For our investigation we assembled a custom-technology SPAD and a recently developed AQC in a prototype detection head that allowed us to operate them at the best of their performance. The detector, developed by using the silicon technology described in [12], has a circular active area with a diameter of 50 µm. The AQC was fabricated on a different

Manuscript received September 30, 2017; revised November 30, 2017; accepted January 10, 2018. Date of publication January 12, 2018; date of current version January 30, 2018. *(Corresponding author: Francesco Ceccarelli.)*

The authors are with the Dipartimento di Elettronica, Informazione e Bioingegneria, Politecnico di Milano, 20133 Milano, Italy (e-mail: francesco.ceccarelli@polimi.it).

Color versions of one or more of the figures in this letter are available online at http://ieeexplore.ieee.org.

Fig. 1. Detection head employed in the experimental characterization.

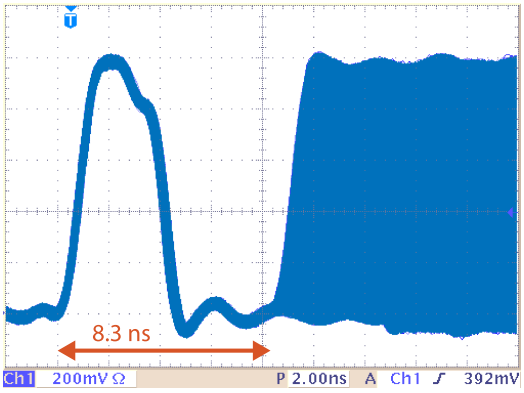

Fig. 2. Output of the module acquired with a digital oscilloscope. The minimum time span between two pulses is 8.3 ns.

chip by using a 0.18-µm high-voltage CMOS (HV-CMOS) technology from Austriamicrosystems (ams H18) [13]. The circuit was specifically developed to drive custom-technology SPADs, either with standard [12] or red-enhanced sensitivity [9] (the latter requiring a voltage swing of up to a few tens of Volts), at high speed. To this aim, the circuit features a sense stage that promptly senses the avalanche current and provides a fast initially-passive quench of the device. High-conductivity HV-MOSFETs are used to rapidly carry out the active part of the quenching phase and the fully-active reset transition. In [13] we demonstrated a dead time as low as 10 ns, when the AQC is connected to a standard sensitivity SPAD.

To minimize the parasitics, the detector and the AQC have been placed in close proximity and the SPAD anode has been connected to the AQC with a direct, chip-to-chip wire-bonding. To exploit the significant reduction of the DCR at low temperatures, the SPAD and consequently the AQC, have been mounted on top of a Peltier thermoelectric cooler. This assembly has been placed in a 12-pin TO package, and sealed in a dry nitrogen atmosphere to avoid moisture condensation during the operation at low temperatures. Fig. 1 shows a top view of the detection head in which is clearly visible the TO package, with the glass window to provide optical access to the detector. The black aluminum case is used as a heat sink for the power dissipated by the Peltier cooler. The TO package is connected to a PCB, located beneath the aluminum case, for an easy routing of the electrical connections. In particular, all the voltages needed for the proper operation of the AQC are provided by external power supplies. The Peltier is actuated by an external instrument (SE5020 by Marlow Industries) that implements also a closed-loop temperature control, thanks to a thermistor placed inside the TO package, in good thermal contact with the SPAD chip. The AQC provides an electrical pulse synchronous with the detection of each photon.

III. Experimental Characterization

We performed an extensive experimental characterization of the detection head. All the results reported in the following sub-sections have been obtained with the detector operated at a temperature $T = -20$ °C and with an excess bias $V_{ex} = 5$ V. These values have been chosen as a good trade-off between DCR, PDE and afterpulsing.

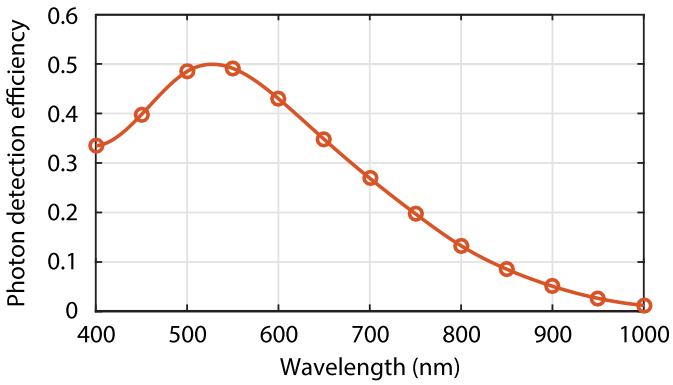

Fig. 3. PDE of the SPAD for a wavelength ranging from 400 to 1000 nm.

A. Dead Time

In order to measure the dead time of the module we used a digital oscilloscope (Tektronix TDS3032B - 300 MHz, 2.5 Gsample/s). The oscilloscope has been triggered on the output signal, and the corresponding waveforms have been acquired with infinite persistence. Results reported in Fig. 2 show that the AQC can actually generate a second pulse as soon as 8.3 ns after the first pulse. To the best of our knowledge, this value represents the shortest dead time achieved so far with a fully integrated AQC that operates an external SPAD. It is worth noting also that this value is considerably lower than the dead time of 10 ns achieved previously with the same AQC [13]. This reduction is mainly due to the fact that the AQC is now operated at $T = -20$ °C, being mounted right beside the SPAD, on the Peltier cooler.

B. Photon Detection Efficiency

The PDE of the module has been measured by using a standard setup based on a monochromator and an integrating sphere, as described in [11]. Fig. 3 reports the attained PDE as a function of the wavelength. The PDE reaches a peak value of 50% at a wavelength of about 550 nm and drops to about 13% at 800 nm. These results are in good agreement with those previously reported in literature for the same type of device [12].

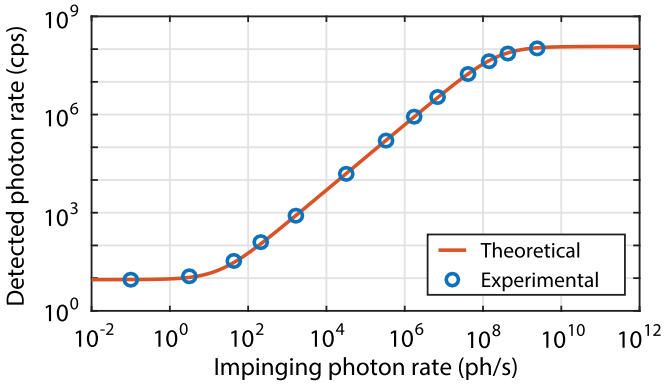

Fig. 4. Linearity curve for the SPAD operated with the new AQC. The maximum achievable count rate is limited to 120 Mcps by the dead time, while the minimum count rate is limited by the DCR at 9 cps.

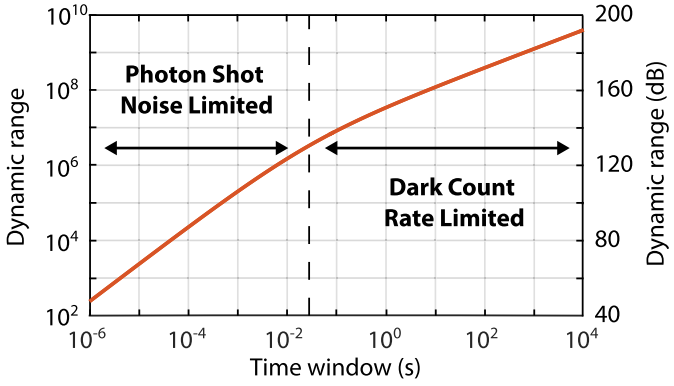

Fig. 5. Plot of DR as a function of the integration window T_w. The dashed line reported on the plot separates the two different regimes.

C. Linearity

In order to verify the actual capability of the detection head of operating at different count rates, we investigated the relation between the number of detected events and the number of photons impinging on the active area. The solid line in Fig. 4 represents the theoretically expected behavior, calculated as described in [11]. It is possible to recognize three different regions: at intermediate photon rates, the relation is linear, with a slope given by the PDE at the considered wavelength λ = 550 nm; at low photon rates, the number of detected events is dominated by the DCR = 9 cps and is therefore constant; at high photon rates, the progressively increasing chance that a photon hits the detector during the dead time, results in a sub-linear relations that eventually saturates at a value given by the inverse of the dead time, i.e. 120 Mcps.

The experimental values reported in Fig. 4 (open circles) have been measured by using the same set-up previously employed for measuring the PDE. In particular, the number of detected events has been measured at different illumination levels, obtained by changing a neutral density filter and the distance from the sphere. The almost perfect agreement between the experimental and theoretical behavior confirms that the detection head operates properly over an extended counting range without introducing any artifacts or distortions (apart the obvious ones related to the DCR and dead time).

D. Dynamic Range

The DR can be calculated as the ratio between the maximum count rate achievable by the detector, n_{sat}, and the minimum photon-induced count rate that can be distinguished from the noise, $n_{ph}|_{min}$. The latter can be obtained as the value of n_{ph} that gives a signal-to-noise ratio SNR equal to 1:

$$SNR = \frac{n_{ph} T_w}{\sqrt{(n_{ph} + n_d) T_w}} = 1, \tag{1}$$

where n_d is the DCR and T_w is the integration window. By solving Eq. 1 for $n_{ph}|_{min}$ and using the obtained value for the calculation of DR we get:

$$DR = \frac{n_{sat}}{n_{ph}|_{min}} = \frac{2 n_{sat} T_w}{1 + \sqrt{1 + 4 T_w n_d}}. \tag{2}$$

Fig. 5 reports DR as a function of T_w, calculated from Eq. 2 with n_{sat} = 120 Mcps and n_d = 9 cps. It is possible to distinguish between two different regimes. For sufficiently small integration windows we have that 4 $T_w n_d \ll 1$; in this case $n_{ph}|_{min}$ is limited by the photons shot noise and DR can be approximated as:

$$DR \simeq n_{sat} T_w. \tag{3}$$

On the contrary, for large integration windows 4 $T_w n_d \gg 1$; in this case $n_{ph}|_{min}$ is limited by the shot noise of the dark counts and DR can be approximated as:

$$DR \simeq \frac{n_{sat} \sqrt{T_w}}{\sqrt{n_d}}. \tag{4}$$

In the literature [5] and [6] the DR is commonly calculated for an integration window T_w = 1 s and expressed in decibel. Using Eq. 4, in this case we obtain:

$$DR = 20 \log \frac{n_{sat} \sqrt{1\ \mathrm{s}}}{\sqrt{n_d}} = 152\ \mathrm{dB}. \tag{5}$$

To the best of our knowledge, this is the highest value reported so far in literature for a SPAD.

E. Afterpulsing

In SPAD detectors there is a probability that, during an avalanche, a carrier gets trapped in a deep level. If the trapped carrier is released when the detector is biased above breakdown, it can trigger a secondary avalanche that is correlated to the first one [12]. This phenomenon is known as afterpulsing and it is usually quantified by means of the afterpulsing probability (AP), defined as the probability of having a secondary pulse given a primary pulse. The afterpulsing phenomenon can be especially detrimental in those applications that require to measure the temporal correlation between photon arrivals, like fluorescence correlation spectroscopy (FCS) [2]. These applications usually require an AP at most of a few percent. Given a SPAD, the AP can be reduced by increasing the amount of time for which the AQC keeps the detector under breakdown (i.e. the hold-off time), as the carriers released in this time span do not trigger an avalanche.

The device under test operates in conditions that are especially harsh from the point of view of the afterpulsing.

TABLE I

COMPARISON AMONG THE PRESENTED DETECTION HEAD AND THE BEST WORKS TO DATE

Detector	Diameter (μm)	PDE (%)			DCR (cps)	Max count rate (Mcps)	Dynamic range (dB)	Afterpulsing (%)
		400 nm	550 nm	800 nm				
0.13-μm CMOS SPAD [5]	8	n.a.	n.a.	n.a.	410	185	139	1.3
0.35-μm CMOS SPAD [6]	20	50	34	5	25	50	140	1.3
8×8 custom array [11]	50 each pixel	22	49	13	33470*	2130	141	∼ 1
This work	50	33	49	13	9*	120	152	2.0

* Thermoelectrically cooled at T = -10 °C [11] and T = -20 °C (this work).

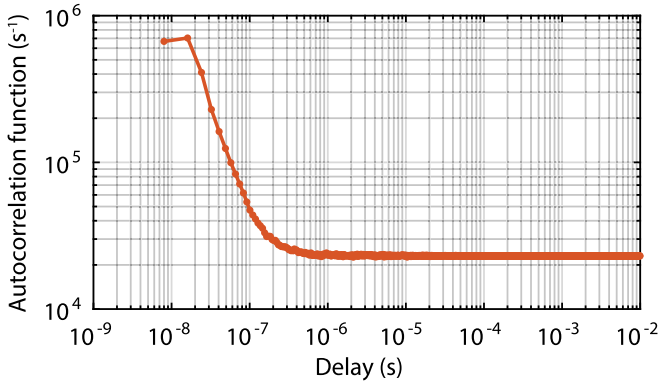

Fig. 6. ACF calculated on the timestamping data. The total AP is 2.0%.

In fact, the fraction of trapped carriers that are released during the hold-off is low, not only because the hold-off itself is especially short, but also because the detrapping rate is reduced by the low temperature at which the device is operated. For this reason it is especially important to quantify the AP of this module. In order to measure the AP, we resorted to an FPGA-based, in-house developed, time-stamper. The time of arrival of each and every photon is recorded with a resolution of 8 ns and the data stream is downloaded to a PC through an USB link. Fig. 6 reports the autocorrelation function (ACF) calculated from the data stream. As a matter of fact this curve represents the average count rate as a function of the delay τ from a generic pulse. For delays longer than a few microseconds, the curve is completely flat indicating no correlation between events; in this region the value is equal to the count rate induced on the detector by an external source of light (that we used to speed-up the measurement). On the contrary, for shorter delays the count rate is higher due to the afterpulsing events that add up to the dark- and light-induced events. By subtracting from the ACF the constant contribution due to primary events we attain the afterpulsing probability density, whose integral is the AP [14]. By performing this calculation on the data of Fig. 6 we attained an AP = 2.0%.

IV. CONCLUSION

The DR of a SPAD-based photon-counting system can be certainly increased by sacrificing other SPAD parameters. For example, the DR can be increased by reducing the V_{ex} and correspondingly the DCR. However, this results also in a reduction of the PDE. Similarly, a reduction of the temperature is beneficial for the DCR but detrimental for the AP. Finally, a reduction of the dead time increases the maximum count rate, but again negatively affects the AP. We demonstrated a record DR of 152 dB, as well as an excellent value for other parameters, in particular a PDE = 50% at a wavelength λ = 550 nm and an AP = 2%. These results compare favorably with the other high-DR SPADs as shown in Table I.

ACKNOWLEDGEMENT

The authors wish to acknowledge P. Maccagnani (IMM-CNR sez. Bologna) for the SPAD fabrication.

REFERENCES

[1] Q. S. Hanley, D. J. Arndt-Jovin, and T. M. Jovin, "Spectrally resolved fluorescence lifetime imaging microscopy," *Appl. Spectrosc.*, vol. 56, no. 2, pp. 155–166, Feb. 2002.

[2] X. Michalet *et al.*, "Silicon photon-counting avalanche diodes for single-molecule fluorescence spectroscopy," *IEEE J. Sel. Topics Quantum Electron.*, vol. 20, no. 6, pp. 248–267, Nov. 2014.

[3] K. J. Gordon, V. Fernandez, P. D. Townsend, and G. S. Buller, "A short wavelength gigahertz clocked fiber-optic quantum key distribution system," *IEEE J. Quantum Electron.*, vol. 40, no. 7, pp. 900–908, Jul. 2004.

[4] C. Vinegoni *et al.*, "Real-time high dynamic range laser scanning microscopy," *Nature Commun.*, vol. 7, Apr. 2016, Art. no. 11077.

[5] A. Eisele *et al.*, "185 MHz count rate 139 dB dynamic range single-photon avalanche diode with active quenching circuit in 130 nm CMOS technology," in *Proc. IISW*, Jun. 2011, pp. 278–280.

[6] D. Bronzi, S. Tisa, F. A. Villa, S. Bellisai, A. Tosi, and F. Zappa, "Fast sensing and quenching of CMOS SPADs for minimal afterpulsing effects," *IEEE Photon. Technol. Lett.*, vol. 25, no. 8, pp. 776–779, Apr. 15, 2013.

[7] D. Bronzi *et al.*, "Low-noise and large-area CMOS SPADs with timing response free from slow tails," in *Proc. ESSDERC*, Sep. 2012, pp. 230–233.

[8] D. Bronzi, F. Villa, S. Tisa, A. Tosi, and F. Zappa, "SPAD figures of merit for photon-counting, photon-timing, and imaging applications: A review," *IEEE Sensors J.*, vol. 16, no. 1, pp. 3–12, Jan. 2016.

[9] A. Gulinatti *et al.*, "New silicon SPAD technology for enhanced red-sensitivity, high-resolution timing and system integration," *J. Mod. Opt.*, vol. 59, no. 17, pp. 1489–1499, Jul. 2012.

[10] C. Cammi, A. Gulinatti, I. Rech, F. Panzeri, and M. Ghioni, "SPAD array module for multi-dimensional photon timing applications," *J. Mod. Opt.*, vol. 59, no. 2, pp. 131–139, 2012.

[11] F. Ceccarelli, A. Gulinatti, I. Labanca, I. Rech, and M. Ghioni, "Giga-count/second photon detection module based on an 8 × 8 single-photon avalanche diode array," *IEEE Photon. Technol. Lett.*, vol. 28, no. 9, pp. 1002–1005, May 1, 2016.

[12] M. Ghioni, A. Gulinatti, I. Rech, F. Zappa, and S. Cova, "Progress in silicon single-photon avalanche diodes," *IEEE J. Sel. Topics Quantum Electron.*, vol. 13, no. 4, pp. 852–862, Jul./Aug. 2007.

[13] G. Acconcia, I. Labanca, I. Rech, A. Gulinatti, and M. Ghioni, "Note: Fully integrated active quenching circuit achieving 100 MHz count rate with custom technology single photon avalanche diodes," *Rev. Sci. Instrum.*, vol. 88, no. 2, p. 026103, Feb. 2017.

[14] M. Zhao, L. Jin, B. Chen, Y. Ding, H. Ma, and D. Chen, "Afterpulsing and its correction in fluorescence correlation spectroscopy experiments," *Appl. Opt.*, vol. 42, no. 19, pp. 4031–4036, Jul. 2003.